Journal of Computer-Aided Molecular Design, 5 (1991) 55–80
ESCOM

J-CAMD 102

On the use of isovalued surfaces to determine molecule shape and reaction pathways*

George D. Purvis III

CAChe™ Group, Tektronix Inc., P.O. Box 500 M.S. 13-400, Beaverton, OR 97077, U.S.A.

Received 5 June 1990
Accepted 30 June 1990

Key words: Molecular reactivity; Electrostatic potential; Gradient mapped electron isodensity; Frontier molecular orbital theory; Orbital interactions; Scientific visualization

SUMMARY

Novel insights into local molecule structure and reactivity can be gained from viewing isovalued surfaces of the molecular electron density, electrostatic potential and molecular orbitals rendered as colored, 3-D objects. For example, drawing positive and negative electrostatic isopotential surfaces partitions the molecule into regions subject to nucleophilic or electrophilic attack. Similarly, coloring isodensity surfaces to indicate the magnitude of the gradient of the electron density maps the molecule surface into regions of high and low electronegativity.

A basic understanding of reaction mechanisms can also come from viewing and manipulating isovalued surfaces. A theory of molecular interactions, based upon second-order perturbation theory, provides for the decomposition of the intermolecular interaction energy into *steric, electrostatic* and *orbital* interactions. Color figures illustrate the docking of reactant molecular densities, electrostatic potentials and orbitals on low-energy pathways. The figures are used to visualize the steric, electrostatic and orbital contributions to molecular interaction energy. The visualization not only identifies low-energy reaction pathways, but it frequently reveals *local* interactions which determine the magnitude of the total interaction energy. Similar insight is not easily obtained by simple evaluation of the total interaction energy. Approximate transition states, built from structures along low-energy approach pathways, are excellent starting points for transition state searches.

1. INTRODUCTION

In the 1980s, computer graphics advanced and matured faster than other computer-based technology. Today, the results of computational chemistry can be calculated, displayed and manipulated just like physical models using graphics-based modeling instruments which are no more expensive than other benchtop chemistry instruments. This new generation of graphics hardware and chemistry software permits real-time, full-color, 3-D stereoscopic display of frontier orbitals,

*CAChe™ Technical Report No. 1, Tektronix Inc., Beaverton, OR.

electron densities, electrostatic potentials and other representations of molecular and electronic structure which are impossible to build using physical models. Colored images of orbitals which, through stereo viewing, appear suspended in space can be docked to simulate reactionlike interactions. Visually manipulating results from computational chemistry on a desktop modeling instrument opens exciting possibilities for exploring chemistry to both the bench chemist and theoretical chemist alike. Using an instrument which produces new data through computational modeling and is capable of stimulating the conceptualization of new experiments offers unique opportunities for major breakthroughs.

Every advance in instrumentation requires time before its proper role is understood and it is assimilated into the workplace. Once upon a time, NMRs, GCs and even IRs were relegated to central instrumentation laboratories. Today, they are accepted benchtop equipment. The role of the computer as a data repository for chemical structures and reactions is likewise becoming an accepted standard. Someday soon, modeling instruments will be accepted as valuable tools used at the conceptualization, hypothesis formation and reporting stages during the process of creating molecules by design. At that time, modeling instruments will become as pervasive on the benchtop as GCs and IRs.

Historically, new technologies have advanced science by automating methods which were too cumbersome for widespread use. For example, commercial laboratory infrared spectrophotometers no longer require labor-intensive hand recording of absorption at each wavelength but instead plot absorption automatically. The simple volume of data generated in quantum chemistry calculations have limited widespread use. Since visually based modeling can simplify both the use and interpretation of quantum chemistry, a revolution in the way computational chemistry is used is pending.

In this paper, advanced computer graphics are applied to display molecular electronic properties, interactions and reactions. The following section explains the general problem of visualizing electronic properties. The next three sections describe the display of molecular orbitals, molecular electron density and electrostatic potential. Then, a simple theory of molecular interactions based upon second-order perturbation theory of molecular orbitals is reviewed. This theory decomposes the intermolecular interaction energy into steric, electrostatic and orbital interactions.

The final section shows how displays of molecular densities, electrostatic potentials and orbitals are used to visualize the three contributions to molecular interaction energy: steric hindrance, electrostatic attraction or repulsion and orbital interaction. Visualization provides qualitative insight into the contributing pieces of the interaction energy. This insight is not easily obtained by simple evaluation of the total interaction energy.

2. THE SHAPE OF MOLECULES

The distribution of electrons in molecules and the response of these electrons to perturbations determine the physical and chemical properties of molecules. Because electrons are fundamental to chemistry, display of electronic structure and response – which lead to the understanding of electrons in molecules – can be crucial to the interpretation of chemistry and design of molecules.

The wave-like distribution of electrons in molecules is completely described by the Schrödinger equation. The work of computational quantum chemists during the past sixty years has focused upon the solution of this intractable multi-dimensional differential equation. Solutions of this

equation for each molecular state define the shape and extent of the electron cloud. Each solution is a complex mathematical function, called the wavefunction, which depends upon the coordinates of all the electrons and nuclei in the molecule. The widespread use of quantum-chemical calculations today attests to the comparative ease with which chemists can solve the Schrödinger equation. In spite of the relative ease with which wavefunctions are found, the complexity, which arises from a function that requires three coordinates for each electron and nucleus, remains. To be specific, the molecular wavefunction, Ψ, has three Cartesian coordinates, r = (x,y,z), for each of the n electrons and N nuclei in the molecule: $\Psi(r_1, r_2,..., r_n; R_1,..., R_N)$. Even methane, which has ten electrons and five nuclei, has a wavefunction of 45 Cartesian variables*. Fortunately, most of the time only the average properties are needed and the electron cloud can be described by the average distribution of electrons, a function of three coordinates at a specified geometry. The average distribution is obtained by integrating $\Psi^*\Psi$ over all but one of the electronic coordinates at a particular molecular geometry. The result is called the electron density [1]:

$$\rho_R(r) = \int \Psi^*\{r; r_2;...r_n; R\}\ \Psi\{r; r_2;..., r_n;R\}\, dr_2... dr_n$$

Here R indicates the nuclear coordinates defining the chosen geometry. $\rho_R(r)$ is the probability that an electron is at position r and it is the quantum mechanical description of the electron cloud for the chosen conformation R.

Even when the description of the electronic structure is simplified so that it is only necessary to render the probable position of an average electron instead of the probable position of each electron, the display of electron position is not trivial. The density is a function of three variables: x, y and z. It might seem that drawing the density as a solid 3-D object would display all of the density information. Such is not the case. Displays of a solid object show its surface. The surfaces of common everyday 3-D objects, like balls and sticks, are parametric functions of two variables while the electron density is a function of three variables. To avoid loss of information, a function of three variables, such as ρ, must be displayed as a volume-filling cloud, or as the surface of a 4-D object. Since rendering and interactive manipulation of a volume-filling cloud is neither widely available nor easy to interpret, it is helpful to reduce the dimensionality so that ρ can be easily rendered and understood. The following paragraph explains a method for rendering the surface.

The use of molecular models has trained chemists to think of molecules as solid, 3-D objects. Thus, simplifying the display of the electron cloud so that it appears as though it were the surface of a complicated 3-D object seems natural. Such a surface is produced by showing all points in the electron density with a specified value, $\rho(r;R) = C$. Because every point on the drawn surface has the same value, it is called an *isovalued surface*. An isovalued surface can define the shape of a molecule. For example, because the surface generated by an isodensity of 0.002 a.u. (1 a.u. = 6.748 e/Å^3) yielded dimensions in agreement with kinetic theory data, the 0.002 a.u. isodensity surface has been used to define the van der Waals envelope of a molecule [2] and thereby its shape. The algorithms for displaying isovalued surfaces have been described elsewhere. [3–5].

Clearly, when this style is used some information is lost. An isovalue drawing of a cloud provides no clue as to the shape of the cloud at other values. This is not as limiting as it might seem.

*This count assumes that the center of mass and rotational degrees of freedom have not been separated out.

Information lost by displaying only an isovalued surface can be partially restored by coloring the surface with colors which indicate the rate of change of the function. In other words, the surface is colored by the magnitude of the gradient. Of course, the gradient of a function at a point is a vector and a complete rendering requires that its direction be indicated. Since the gradient of an isovalued surface is always perpendicular to the surface, the color and the curvature of the surface together provide a complete encoding of its rate and direction of change (the so-called surface gradient vector field). This allows the viewer to estimate the shape at different isovalues. The color coding also provides information about the electronic structure which can help with the interpretation of particular molecular properties.

Although it is tempting to think that a picture of the molecular electron cloud is the only, or the best, picture of the molecule's shape, such is not the case. Like all properties of molecules, information about molecular shapes comes from measuring the response of probes, e.g. X-rays, which are projected at the molecule. Because different probes generate different responses, the shape depends on the probe. An X-ray crystallographic experiment maps the molecular electron density. On the other hand, angle-resolved photoelectron spectroscopy maps molecular orbitals while electron scattering and proton scattering experiments map the molecular electrostatic potential [6]:

$$V(r) = -\int \frac{\rho(r')}{r - r'} dr' + \sum_i \frac{Z_i}{r - R_i}$$

Thus, the shape of a molecule derived from experimental data depends upon the probe used to map the molecule. Likewise, the molecular shape required to interpret experimental data depends upon the experiment performed.

The next three sections discuss isovalued renderings of molecular orbitals, electron densities, and electrostatic potentials: three different views of molecules.

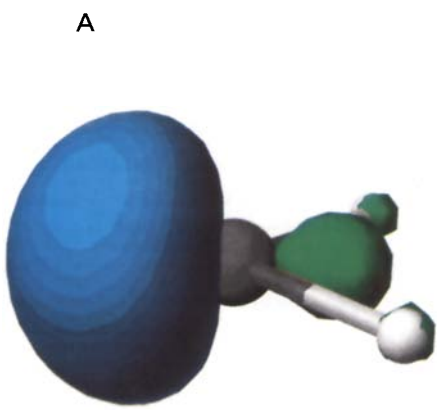

Fig. 1A. Methylene $3a_1$ orbital.

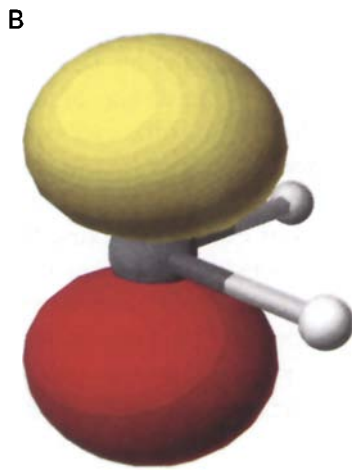

Fig. 1B. Methylene $1b_1$ orbital.

Molecular orbitals

Orbitals are one-electron wavefunctions. Orbitals are the product of both a spatial function and a spin function. Since the α- and β-spin functions are orthogonal, two electrons can have the same spatial part. Orbitals, rather than densities, are central to models of electronic structure and bonding because the interference effects of quantum mechanics arise from superimposing orbitals. Orbitals interfere when negative lobes of one orbital cancel positive lobes of another orbital.

As a result of the central role of molecular orbitals in explaining chemical bonding, few chemists will fail to recognize the isoamplitude surface [7] of the methylene $3a_1$ lone-pair orbital shown in Fig. 1A. The blue lobe is the 0.2 a.u. isoamplitude surface and the green lobe is the -0.2 a.u. isoamplitude surface. The 0.2 isoamplitude surface displays those points where the probability amplitude is 0.2 a.u. The square of the probability amplitude yields the probability.

The $3a_1$ orbital is the highest occupied molecular orbital (HOMO) in the $^1A_1$ state of methylene. The lowest unoccupied molecular orbital (LUMO) is the $1b_1$ orbital shown in Fig. 1B. The red (yellow) lobe is the 0.2 (-0.2) a.u. isosurface. The methylene orbitals are contoured at the 0.2 level to show the principal atomic orbital contributions to the molecular orbitals.

Molecular orbitals have small contributions from all atomic orbitals with appropriate symmetry. In large molecules, even localized orbitals have many small contributions from remote atomic orbitals and they are never as localized as they would be in a small molecule. Thus, for a fixed contour level, the volume enclosed in the orbital isosurface decreases with molecule size. The best contour level for a particular molecule depends upon the number of electrons in the molecule and the delocalization of its orbitals. For molecules containing more than ten electrons but fewer than 30 electrons, a 0.1 a.u. amplitude is a good choice. For molecules containing more than 30 electrons, a 0.07 a.u. amplitude is a good choice [5]. For those with more than 60 electrons, a 0.05 a.u. amplitude is good. Contours of the total electron density, discussed in the next section, do not have this problem, because the total number of electrons increases with molecule size.

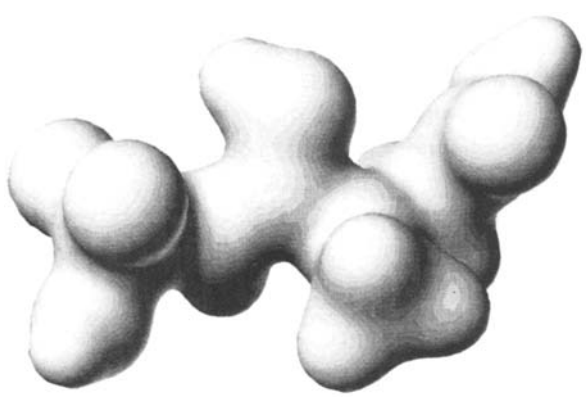

Fig. 2. The MNDO 0.05 a.u. isodensity surface of phosphocreatine.

TABLE 1
GRADIENT COLOR SCALES

Contour	Gradients							
		P	C	H	N	O	F	
(a.u.)	Yellow	Violet	Grey	White	Blue	Red	Green	Cyan
0.010	0.014	0.021	0.026	0.033	0.040	0.044	0.055	
0.020	0.028	0.040	0.050	0.058	0.071	0.087	0.100	
0.040	0.056	0.080	0.097	0.112	0.150	0.170	0.200	
0.080	0.080	0.130	0.180	0.230	0.270	0.325	0.380	

The electron density

The electron density of ground states

Because electrons are fundamental to chemistry and because the electron density is the probability of finding an electron at any point around the molecule, its picture ought to deliver immediate insight into molecular structure. Figure 2 shows the MOPAC [8] calculated MNDO [9] 0.05 a.u. electron isodensity of phosphocreatine at the optimized geometry.

The picture is remarkable, not for what it shows, but for what it does not show. In spite of the fact that it summarizes the result of a substantial calculation of a many-electron wavefunction, it is devoid of interesting chemical detail. With great difficulty, the smaller bumps might be identified as hydrogen atoms, but distinguishing the carbon, nitrogen and oxygen atoms is nearly impossible. Even the phosphorous atom is difficult to identify. The space-filling ball model in Fig. 3 is clearly more useful. A moment's glance reveals the underlying atomic structure which, in turn, provides chemists with immediate insight into the localized properties and reactivities of phosphocreatine. The expectation is that the electron density should provide even more information, including subtle shifts arising from electronegativity differences or multiple bonding.

Figure 4 again shows 0.05 a.u. electron isodensity of phosphocreatine, but this time the surface is colored with the magnitude of the gradient of the electron density. The color scale is given in Table 1*. Color coding the gradient of the electron density clearly displays the underlying atomic structure and the result is a quantum mechanical analogue of a CPK ball model. Linear interpolation is used to find color scales at any other contour level.

Figure 4 shows an obvious relationship between the magnitude of the electron density gradient at a point on the surface and the nearest nucleus. A qualitative explanation can be given. Let the atomic covalent radius be a measure of the size of an atom. From left to right in each row of the

* Although the use of a visible spectrum color scale (red-orange-yellow-green-blue-indigo-violet) is an obvious choice, experience has shown that the spectral scale, compared to the CPK scale used here, obscures the underlying atomic structure without making the magnitude of the gradient significantly easier to read. Chemists have found the CPK scale easy to learn.

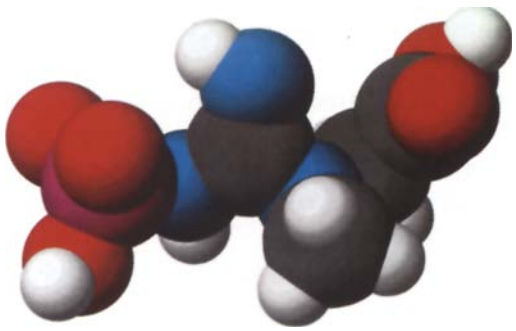

Fig. 3. Space filling ball model of phosphocreatine (0.7 times van der Waals radii).

Fig. 4. Gradient colored 0.05 a.u. isodensity surface of phosphocreatine.

periodic table, covalent radii decrease. Thus, C(0.77 Å) > N(0.75 Å) > O(0.74 Å) > F(0.72 Å) and Si(1.15 Å) > P(1.11 Å) > S(1.04 Å) > Cl(1.00 Å) [10]. On the other hand, the number of electrons in each atom increases from left to right in a row. Consequently, the average density of $e/Å^3$ in an atom whose size is proportional to its covalent radius increases: C(3.14) < N(3.96) < O(4.71) < F(5.76) and Si(2.19) < P(2.62) < S(3.40) < Cl(4.53). Electron densities of neutral atoms are zero infinitely far from the nucleus and they rise monotonically [11] to larger values at the covalent radius of atoms on the right-hand side of the periodic table than for those on the left. The simplest explanation is that the average electron density gradient for an element increases from left to right in the periodic table. This trend was confirmed by a series of calculations on hydrides reported previously for INDO [12] and ab initio wavefunctions [13, 14].

Since the electron density gradient is a continuous function, bonds connecting two different

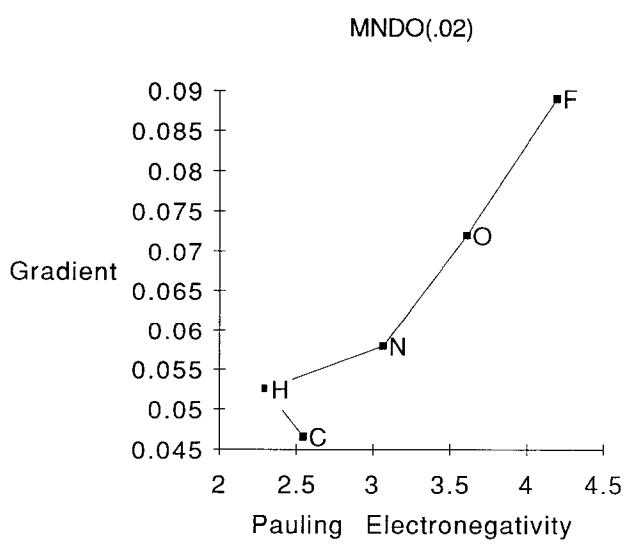

Fig. 5. Average atomic MNDO 0.02 isodensity gradient vs. Pauling electronegativity.

atoms are banded with colors mapping gradients between those of end atoms. For example, a C–O bond always has white and blue bands around itself. If the bond is stretched, then additional colors can band the bond.

While it is obvious from the definition of a gradient that the electron gradient measures the rate of change of the isodensity surface, the relationship of the gradient to atom type just shown is less obvious. There are additional properties whose values can be estimated from the density gradient. As explained in the Appendix, gradient color patterns also measure local ionization potential and the local electronegativity (see Fig. 5).

To see an example of how gradient-colored isodensity surfaces provide more information than just the underlying atomic structure, look at the triangular white patch on the carbon atom at the center of Fig. 4. This central carbon, which is double-bonded to the NH group, is clearly different from the methyl carbon. The triangular white patch indicates a region with higher electronegativity. The central carbon has higher electronegativity, because the attached N atoms have withdrawn electrons leaving a positive partial charge. For the same reason, there is a similar triangular white patch on the carboxylate carbon atom.

The electron density of unconventional bonds

Gradient-colored isodensity surfaces depict underlying atomic structure. Isodensity surfaces also reveal unconventional bonding structures. Consider [1.1.1] propellane [15] shown in Fig. 6. The ball-and-stick model shows the MNDO optimized geometry of [1.1.1] propellane and the calculated bond orders. The radius of the bonds indicates the MNDO bond order. The bond shown in green between the bridgehead 1 and 3 carbon atoms is controversial [16]. The distance between the bridgehead carbon atoms is 1.54 Å, a distance which indicates that there is a C–C single bond. If that is the case, then the bridgehead atoms have four single bonds arranged in an inverted tetrahedron, an unusual configuration for carbon.

Distance between atoms is only one of several criteria for assigning bond types. A second criterion for a normal C–C bond is a buildup of charge between the atoms. Note that the bridgehead bond radius (Fig. 6) is visibly smaller than that of the other C–C bonds. Experimental and theo-

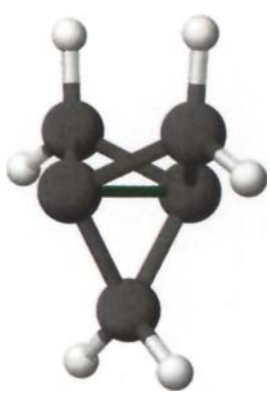

Fig. 6. [1.1.1] Propellane MNDO structure. Bond radii are proportional to bond orders.

Fig. 7. The MNDO 0.09 a.u. isodensity of [1.1.1] propellane colored by the magnitude of the electron density gradient.

Fig. 8. MNDO 0.02 a.u. isodensity of [1.1.1] propellane colored by the magnitude of the electron density gradient.

retical deformation density plots have shown that there is a decrease in total charge between the bridgehead atoms, indicating that a conventional C–C single bond is absent.

Jackson and Allen [16] have proposed that the distance between the bridgehead carbon atoms is short because the bridgehead carbons participate in a unique three-center σ-bridged π-bond and not an axial bond. This bond is made up of the 2pπ C_2 fragment orbitals on the bridgehead carbons and the sp^2 lone pairs of the methylene bridges. Gradient-mapped isodensity surfaces provide supporting evidence for this interpretation of bonding in [1.1.1] propellane.

Figure 7 shows the gradient mapped 0.09 a.u. isodensity surface of [1.1.1] propellane. Note the purple dimple in the isodensity surface in the region of the bridgehead C–C bond. The hole in the center of the molecule is counter to the expectation that the electron density increases between the atoms in a C–C single bond. The purple gradient indicates that the rate of change of the electron density in this bond region is much slower than the rate of change around a typical C–C bond. Thus, the 0.02 isodensity surface shown in Fig. 8 has a purple region, but the dimple is no longer prominent.

A second characteristic of the unconventional bond is the change in the electron distribution around the bridgehead atoms. The larger size of the bridgehead atoms compared to the methylene carbon atoms is consistent with the −0.12 atomic charge and the 2pπ bond formed. As can be seen in both Figs. 7 and 8, the electron distribution on the backside of carbon is shifted from charcoal to white, indicating a greater rate of change of the electron density, a greater local electronegativity and more tightly held electrons. In short, the bridgehead carbon atoms look very much like the carbon atom in the $^3B_1$ state of methylene shown in the next section (see Fig. 11) demonstrating occupancy of the 2pπ orbitals on the bridgehead. The absence of charge buildup along the bridgehead axis and the occupancy of the 2pπ orbitals on the bridgehead support the concept of a three-center bond in [1.1.1] propellane. This information could also be derived from deformation densities but derivation from the gradient colored density avoids the pitfalls associat-

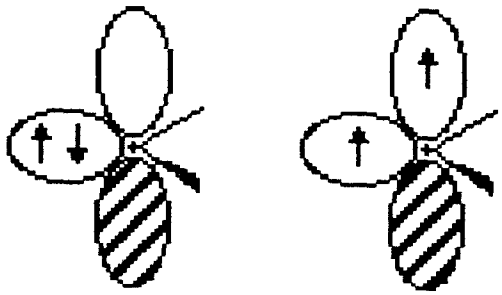

Fig. 9. The $^1A_1$ (left) and $^3B_1$ (right) states of methylene.

ed with the assigning of the standard atom densities of open-shell atoms required for calculation of a deformation density.

The electron density of excited states

The electron density can be rendered so that the intrinsic atomic structure is visible. This rendering can also reflect the total electronic state [5].

From the perspective of graphical display, the total electron density is notoriously uninteresting, primarily because it seems to lack structure. Consequently, molecular orbital probability amplitudes have been a principal vehicle for visualizing electronic structure. However, molecular orbital amplitudes, unlike the electron or orbital density, are not physically observable. Furthermore, orbitals are not unique since any unitary transformation of a set of occupied molecular orbitals produces a new valid set of orbitals. Thus, it is valuable to reexamine the display of electron density to see if it can, after all, indicate the molecular electronic state.

Consider the $^1A_1$ and $^3B_1$ states of methylene. The $^1A_1$ state of methylene contains a doubly occupied $3a_1$ orbital and an unoccupied p_z-like $1b_1$ orbital perpendicular to the CH_2 plane while the $^3B_1$ state has an electron in each orbital (Fig. 9).

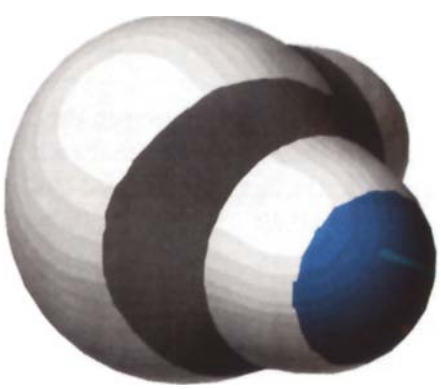

Fig. 10. The 0.09 a.u. isodensity of the $^1A_1$ state of methylene.

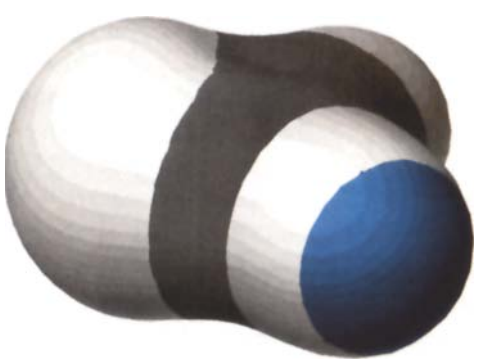

Fig. 11. The 0.09 a.u. isodensity of the $^3B_1$ state of methylene.

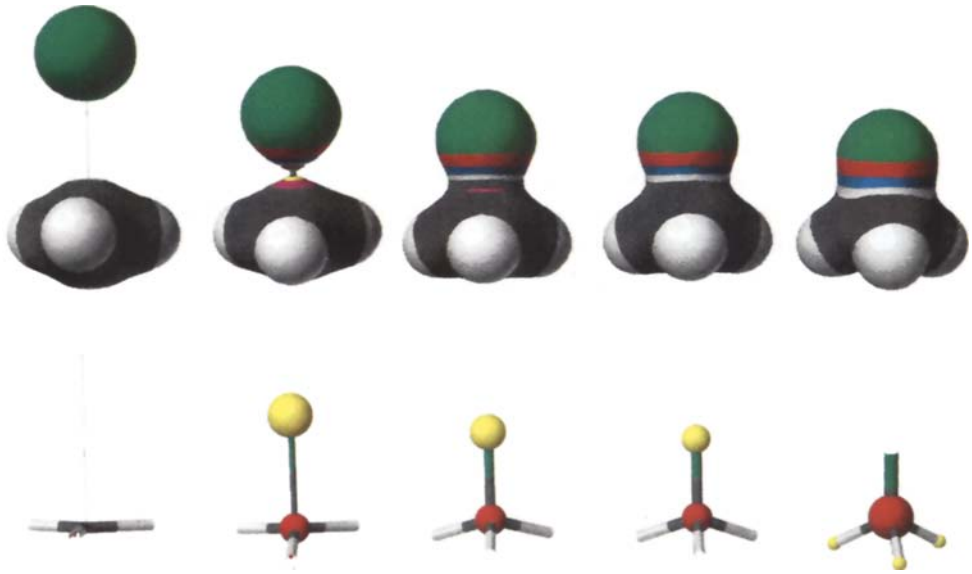

Fig. 12. The sequence of pictures shows the MNDO isodensity surfaces (top row) and partial charges and bond orders (lower row) for the stepwise approach of F to methyl radical during the formation of methyl fluoride. The F to C distance is 3.0 Å, 2.0 Å, 1.5 Å; $R_e = 1.347$ Å, 1.0 Å.

Figures 10 and 11 show the MNDO 0.09 isodensity surfaces of the $^1A_1$ and $^3B_1$ states of methylene. Although the effect is modest, the bulge in the isodensity plot of methylene behind the carbon atom (Fig. 10) clearly shows a buildup of electrons in the region of space where the $3a_1$ orbital is located. The depression in the isodensity plot above the $^1A_1$ carbon atom indicates an absence of electrons in that region.

It is interesting to see the magnitude of distortions in the electron density induced by the electronic configuration. The shape of molecules as defined by the total electron density can be visibly altered by the electron configuration.

The electron density during a chemical reaction

The sensitivity of molecular isodensity surfaces to electronic structure suggests that displays of isodensity surfaces along a reaction path will be informative [14]. Figure 12 displays the change in the total electron density of CH_3F as a fluorine atom moves along the reaction pathway from 3 to 1.0 Å (optimized MNDO $R_e = 1.347$ Å).

The MNDO density was calculated using MOPAC. Points between 1.0, R_e and 1.5 Å were based upon the restricted Hartree–Fock (RHF) wavefunction. The points between 2.0 and 3.0 Å used a spin unrestricted Hartree–Fock (UHF) reference function.

The colors on the isodensity surface map the magnitude of the electron density gradient (see Table 1 in the previous section). Notice that at large separation, the fluorine atom is a green sphere which gradually distorts and becomes banded as it reaches the equilibrium distance. As fluorine is pushed inside of the equilibrium distance, the density in the C–F bond builds.

The colors indicate that, at long separation, the gradient of the fluorine atom electron density is similar to that of free fluorine. As the bond between fluorine and carbon begins to form, electron density flows into the space between the fluorine and carbon and the gradient bands around the C–F bond widen. Note that although electrons are shifted during the reaction, changes in atom sizes are small but the changes in the gradient patterns are noticeable. Thus, the gradient of the electron density is a sensitive indicator of changes in bonding. This illustrates that gradients of the electron density are sensitive to the local chemical environment and can be used to highlight subtle changes in chemical bond formation.

The highlighting of unusual bonding structures is especially important in larger molecules where the large number of bonds may hide the interesting bonds. For example, look at the purple area in phosphocreatine (Fig. 4) around the methyl C–N bond. The bond order is 0.91, significantly weaker than a normal single bond order of 0.97–1.0. Similarly, the purple-banded single bonds around phosphorous have bond orders of 0.75.

Electrostatic potentials

Electrostatic potential of ground state molecules

The molecular electrostatic potential is the energy of interaction of a free proton with a molecule. The magnitude and sign of the energy is an indication of the molecule's susceptibility to electrophilic attack [17]. A region of the molecule where the electrostatic potential is comparatively large and negative is a region susceptible to electrophilic attack. A region with a large positive energy is subject to nucleophilic attack.

Displaying the electrostatic potential of a molecule by drawing the positive and negative isovalued surfaces partitions the molecule into regions subject to electrophilic and nucleophilic attack. Figure 13 shows the ± 0.05 a.u. (± 31.4 kcal/mol or ± 131.3 kJ/mol) isopotentials for phosphocreatine. The backside of the ± 0.05 a.u. isopotentials is shown in Fig. 14. The blue surface envelops the negative electrostatic potential regions and the red envelops the positive electrostatic potential region. The positive (red) surface encompasses the region subject to nucleophilic attack. The negative (blue) surface encompasses the region subject to electrophilic attack.

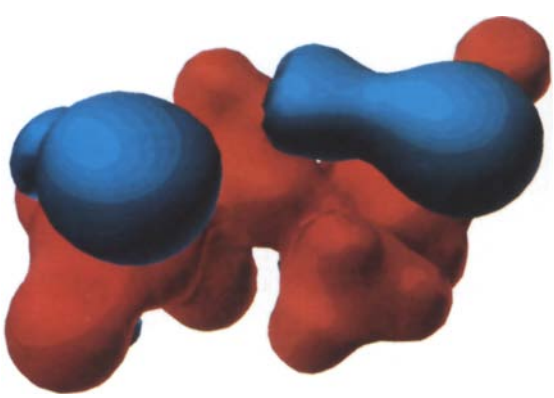

Fig. 13. The ± 0.05 a.u. electrostatic isopotential for phosphocreatine.

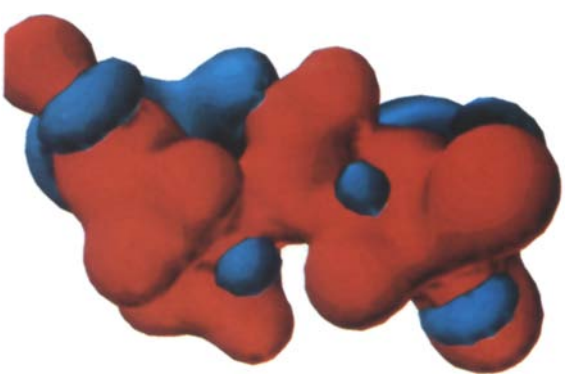

Fig. 14. The ± 0.05 a.u. electrostatic isopotential for phosphocreatine rotated about the y-axis by 180°.

Fig. 15. The transparent (stippled) ±0.05 a.u. MNDO electrostatic isopotential of phosphocreatine superimposed on its 0.03 a.u. MNDO isodensity.

At first glance, it may seem strange that the oxygen and nitrogen atoms are surrounded by the positive surface. Concepts of partial atomic charge have prejudiced our understanding of molecule structure in a peculiar way. The long time habit of writing partial positive and negative charges next to atoms in chemical formulae has led to the concept that the region of partial net charge is at the nucleus. On reconsideration, it is obvious that the region of negative charge is never apt to be at the nucleus, since the large positive charges of the nucleus are there. Thus, the nucleus of every atom, even oxygen and nitrogen, is surrounded by a positive electrostatic potential.

Figure 15 compares the picture of electrostatic potential of phosphocreatine shown in Fig. 14 with its 0.03 isodensity surface (for orientation see the 0.05 isodensity in Fig. 4). There are both similarities and differences. The shape of the isodensity resembles the *positive* electrostatic surface in most places. However, radii of atoms which are positively charged are proportionally larger in the electrostatic representation than in the density representation and those with lone pairs are proportionally smaller. Similarly the radii of atoms which are negatively charged are proportionally smaller in the electrostatic representation.

There are no shapes generated by the isodensity which are similar to the shape of the negative isopotential surfaces. Negative isopotential surfaces usually appear in the region of lone-pair electrons or near π bonds. Minima in the electrostatic potential are approximately located near the centers of volumes enclosed by negative isopotential surfaces. They are at least 1Å away from the nearest nucleus in the direction of a lone pair or π bond. A classic example of the negative potential associated with π bonding is shown for benzene in Fig. 16.

Electrostatic potential of excited states

While it is well-known that the electrostatic potential defines a molecular shape which is significantly different from the shape defined by simple ball models, it is less well-known that the excited-state electrostatic potential has its own characteristic shape.

The characteristic signature of the electrostatic potential of the $^1A_1$ and $^3B_1$ methylene states is

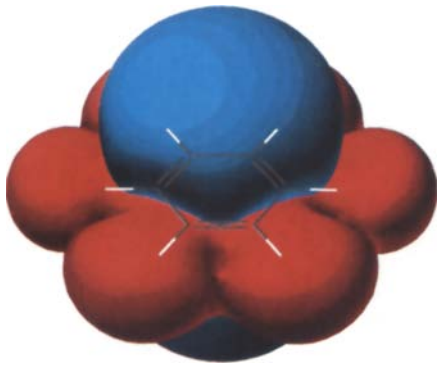

Fig. 16. The AM1 ± 0.01 a.u. electrostatic isopotential of benzene. Note the presence of a large negative potential above the benzene ring.

displayed in Figs. 17 and 18. Note the large negative lobe in Fig. 17 to the left of the carbon atom. This lobe comes from the occupied $^1A_1$ lone pair (see Fig. 9). Note the positive electrostatic potential extends perpendicular to the CH_2 plane because there are no electrons in the empty $1b_1$ orbital to shield the nucleus.

The ± 0.03 a.u. (18.8 kcal/mol or 78.8 kJ/mol) electrostatic potential of $^3B_1$ methylene illustrates the more isotropic distribution of electrons in this state which places one electron in the $3a_1$ orbital and another in the $1b_1$ orbital. Clearly, the $^1A_1$ and $^3B_1$ methylene states are differentiated by their electrostatic potentials.

3. VISUALIZING MOLECULAR INTERACTIONS

Although the analyses of chemical reactions using computational chemistry are usually presented in quantitative, numerical terms, qualitative visualizations based upon the shapes of

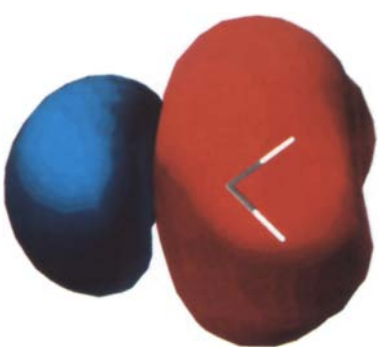

Fig. 17. $^1A_1$ methylene ± 0.03 a.u. electrostatic isopotential.

Fig. 18. $^3B_1$ methylene ± 0.03 a.u. electrostatic isopotential.

densities, electrostatic potentials and orbitals often provide more insight. Understanding reaction mechanisms is a crucial element in deciding how to modify reactants and experimental reaction conditions to achieve particular synthetic goals. The number of possible effects on molecular reactivity, such as solvent and temperature, means that time-consuming quantitative calculations of precise gas phase reaction mechanisms are likely merely qualitative predictors of actual experimental pathways. Fast qualitative reactivity models can provide better insight by focusing on simple components of molecular interactions which can be extended to more complex systems.

Two reactants will produce products only if they find an energetically feasible pathway for reaction. Pathways with favorable interaction energies at long, intermediate and short range ought to be low energy pathways. Isovalued surfaces of molecular electronic densities, electrostatic potentials and molecular orbitals define molecular shapes which can be used to visualize the relative magnitudes of molecular interactions and provide insight into the local interactions which make a reaction pathway favorable or unfavorable. Applying the three-step procedure outlined in the following sections, the relative overlap of reactant orbitals, densities and electrostatic potentials along an interaction path can be used to estimate visually the magnitude of terms in the interaction energy. The graphical visualization of interaction terms emphasizes the qualitative nature of the reactivity model.

A reactivity model

Chemical reactions are controlled by many factors. These factors include the relative abundance of conformations in the reactants, the height of any barriers to the reaction, the shape and width of any transition states, the presence and nature of solvents, the formation of stable reaction intermediates, secondary geometrical changes in the geometry of the reactants as the reaction progresses and also the simple, direct interaction between reactants.

This section develops a mathematical foundation for a *reactivity model* which explains the fundamental interactions between reactants. Subsequent sections describe procedures for visualization of the reactivity model. To the extent that the reaction is dominated by the simple direct interactions between reactants, this reactivity model explains the reaction mechanism and predicts the reaction products. It can also be useful when comparing *differential* reactivity in a sequence of reactions run under identical conditions using different, but similar reactants – even if the reactions take place in solvent. Like the reactivity models developed by others [18], this model is particularly amenable to graphical display.

The model is based upon the simplest molecular orbital theory and, although applied here to small molecules, it is applicable to the explanation of large molecule reactions. Furthermore, it is extensible to the interpretation of more sophisticated quantum chemical methods.

Consider the intermolecular interaction energy $\triangle E_{int}$ between reactants I and II. Incipient interactions of the reactants are initially small perturbations which can be evaluated by perturbation expansions of the wavefunction and energy [19]. Based upon perturbation expressions for the change of energy, $\triangle E$, which happens when orbitals of one reactant overlap the orbitals of another reactant, Klopman [20] and Salem [21], found the interaction energy is composed of three terms which can be called the *steric, electrostatic* and *orbital* terms. Fleming in his book on frontier orbital theory [22] writes an equation for the interaction energy similar to the following and identifies the *steric, electrostatic* and *orbital* interaction terms:

$$\Delta E = -\sum_{pq} (q_p + q_q)\,\beta_{pq}\,S_{pq} \qquad \text{steric}$$

$$+\sum_{A\in I}\sum_{B\in II} \frac{Q_A\,Q_B}{\varepsilon R_{AB}} \qquad \text{electrostatic}$$

$$+\sum_{i\in I}\sum_{a\in II} 2\frac{(\Sigma_{pq} c_{pi}\,c_{qa}\,\beta_{pq})^2}{\varepsilon_a - \varepsilon_i} \qquad \text{orbital}$$

$$+\sum_{i\in II}\sum_{a\in I} 2\frac{(\Sigma_{pq} c_{pi}\,c_{qa}\,\beta_{pq})^2}{\varepsilon_a - \varepsilon_i} \qquad \text{orbital}$$

In the energy expression, q_p is the electron population in atomic orbital p; β and S are the atomic resonance and overlap integrals; Q_A and Q_B are the total net charge on atoms A and B; R_{AB} is the distance between atoms; ε is the dielectric constant; ε_i is the ith orbital energy; C_{pi} is atomic orbital p's coefficient in molecular orbital i; and I, II are reactant molecules I and II.

The *steric* term is a first order term which describes the repulsion between reactants when occupied orbitals on reactant I overlap occupied orbitals on reactant II. Because this term forces electrons from reactant I into space occupied by electrons from reactant II, it is repulsive.

The *electrostatic* term reflects the first-order Coulombic interactions of charged or polar reactants. The electrostatic interaction energy is the energy arising from attraction and repulsions of the net partial charges associated with each atom.

The *orbital* interaction energy (which is valid if $\varepsilon_a \neq \varepsilon_i$) is the energy required, or released, when the electrons from the occupied orbitals of one reactant move into empty orbitals on the other reactant.

Qualitatively, the electrostatic interaction controls the long-range orientation of molecules, the steric interaction prevents the short-range collapse of the reactants and the orbital term allows or disallows bond formation.

Strictly speaking, this equation is valid only for small overlaps, which is true for p-orbitals and for reactions with an early transition state. However, this equation and its classification into three terms can also be derived from a treatment based upon Mayer's chemical Hamiltonian [23] which is valid for both long-range and intermediate-range interactions.

Because steric interaction terms tend to be similar in a homologous series of reactions and because many such series are hydrocarbons without large electrostatic interactions, the orbital term forms the basis of frontier molecular orbital theory [22]. Of course, if the reaction does not break or form bonds (e.g. biomolecular nonbonded interactions) then this term is unimportant and omitted.

Although the molecular interaction energy is composed of three major terms, many successful interpretations of chemical reactions have been based primarily upon orbital interactions [5, 7, 24–27], charge distributions [28], or electrostatics [29, 30]. These methods enjoy success when they are used to explain differences in chemical reactivity within specific classes of reactions where the effects of the other terms are uniform.

A few monographs have been devoted to the use of two of the three major contributors to molecular interactions, for example, orbital and electron densities [31]. Recently, assignments of the observed regioproduct in cycloadditions to dienes substituted by two different groups or by the

same group in different diene positions has been based on the matching of reactivity surfaces for diene and dienophile [18, 32–34]. The reactivity surfaces include a combination of steric and electrostatic interactions by color coding the value of the electrostatic potential on an electron isodensity surface.

Visualizing steric hindrance

The *steric* term is a first-order term which describes the repulsion between reactants when occupied orbitals on reactant I overlap occupied orbitals on reactant II. Because this term forces electrons from reactant I into space occupied by electrons from reactant II and vice versa, it is repulsive. Providing obviously large steric interactions are avoided, this first term – a large, typically repulsive effect – is expected to be comparable for different possible reaction pathways and it does not usually contribute to the differential reactivity.

At any orientation of the reactant molecules, the steric term can be estimated by viewing reactant electron isodensities. The molecular electron density gives the probability that an electron in any occupied orbital occupies a specified small region in space. Thus, simple space-filling pictures of molecular isodensities indicate regions of space where reactants I and II have high electron densities and which should not overlap significantly unless there are large compensating orbital or electrostatic terms.

Two reactants have large steric hindrance if their isodensity surfaces overlap. Clearly, the magnitude of the interaction depends upon both the size of the overlap and the probability value selected for the isodensity surface. For a given set of comparisons, a consistent choice of isovalues must be made. Since an isodensity surface of 0.002 a.u. approximates a van der Waals surface, a 0.002 isodensity surface is appropriate for investigating van der Waals interactions. For estimating steric contributions at the transition state, isodensity values of 0.05–0.01 are useful since they are consistent with the usual choice of 0.1 a.u. for the orbital amplitude.

Visualizing electrostatic attraction and repulsion

The *electrostatic* term reflects the first-order Coulombic interactions of charged or polar reactants. The electrostatic interaction energy is the energy arising from attraction and repulsions of the net partial charges assigned to each atom. This term is zero for nonpolar, uncharged reactants like He, and it is small for alkanes. Depending upon the charge and orientation of the reactants, the electrostatic energy may be negative (a net attractive interaction) or positive (a net repulsive interaction). For example, dipoles oriented so that opposite charges are adjacent have an attractive interaction, while those oriented so that like charges are adjacent have a net repulsive interaction.

The importance of the electrostatic interaction has been emphasized in a recent series of papers [18, 32–35]. Electrostatic interactions between polar molecules are important both because they dominate at long distances and because they are large in the transition state region. The long-range electrostatic interaction of two dipolar molecules [19], varies with the inverse cube of the intermolecular distance R^{-3} while the other terms at long range vary as the inverse sixth power R^{-6}. Since the Coulomb potential decreases with the inverse of the distance between two charges – while the nonbonded repulsion and bonding terms decrease much more rapidly at long distances – electrostatic forces dominate at long range. Thus, electrostatic interactions can be important in determining initial molecular orientation and thereby the channel into which reactants initially

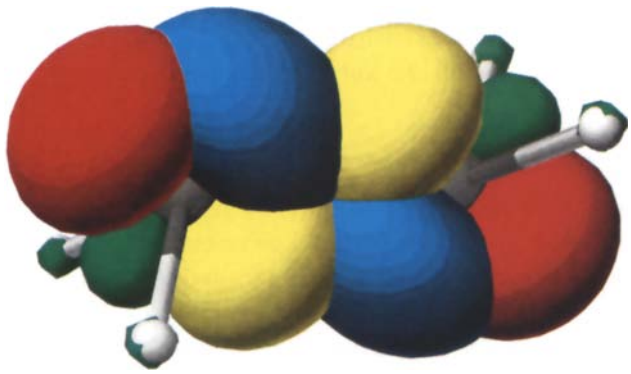

Fig. 19. Approximate reaction pathway point generated by docking the HOMO and LUMO of two methylene fragments. Note the favorable overlap of the HOMO (blue-green) on one fragment and the LUMO (red-orange) on the other.

enter. While the electrostatic term may not contribute to the differential reactivity of nonpolar compounds, it is clearly essential to the interpretation of reactions of polar and ionic species.

A space-filling rendering of reactant electrostatic isopotentials at the interaction configuration allows quick qualitative evaluation of whether a particular configuration is favorable or unfavorable. Electrostatic interactions are reflected in the overlap of the positive and negative isopotential surfaces of reactants. Suggested isopotential values for neutral reactants typically lie in the range of 5–50 kcal/mol (21–209 kJ/mol). Overlaps of positive lobes on one reactant with the negative lobes on the other are favorable. Negative-negative and positive-positive overlaps and adjacencies are clearly unfavorable.

Visualizing orbital interactions

The *orbital* interaction energy is the energy consumed, or released, when the electrons from the occupied orbitals of one reactant move into empty orbitals on the other reactant. Such electron flow is possible when the occupied orbitals on one reactant overlap low-energy unoccupied orbitals on the other and the energy gap is small. Usually, the orbital term is dominated by the interaction of the highest occupied molecular orbital (HOMO) on one reactant with the lowest unoccupied molecular orbital (LUMO) on the other – the frontier orbitals. If the reaction is a dimerization, then reactants are identical and there is no ambiguity in selecting the HOMO or LUMO. In other reactions, the reactants are different and each reactant will have a HOMO and a LUMO. When reactants are different, the orbital term is dominated by the interaction of the HOMO and LUMO with the smallest difference in orbital energy.

Low-energy interactions between two reactants are those where the orbitals overlap constructively. This means that the lobes on the HOMO of one reactant overlap lobes on the LUMO of the other reactant having the same sign. Furthermore, the reactants are oriented to maximize this overlap. Because the sign of any orbital is arbitrary, the sign of all lobes on one of the reactants may be changed to allow the most favorable overlap. An example of a favorable overlap between two methylene fragments is shown in Fig. 19. This figure simultaneously shows the HOMO (blue and green) and the LUMO (red and yellow) on each CH_2 fragment overlapping favorably.

If two orientations have similar orbital overlaps, then the lowest lying, most favorable reaction state must be determined by examination of the steric and electrostatic terms.

Locating reaction pathways

Two reactants will produce products only if they find an energetically feasible pathway for reaction. Pathways with favorable interaction energies at long, intermediate and short range ought to be low-energy pathways. The relative overlap of reactant isovalued surfaces along an interaction path can be used to estimate the magnitude of terms in the interaction energy. Isovalued surfaces of reactants can be displayed and docked graphically to examine overlaps along a reaction pathway, thus providing a visual mechanism for discovering feasible reaction pathways.

In an approximate way, the electrostatic terms control the long-range orientation of molecules, the steric terms prevent the short-range collapse of the reactants and the orbital term governs the transition of bonds.

A simple three-step process can be used to identify energetically feasible pathways. Except in the case of simple donor bonding, product formation requires the breaking and making of electron pairs. Since the term in the reaction model which defines bond making and breaking is the orbital interaction energy, the *first step* in identifying feasible low-energy reaction pathways is to find reactant orientations with large HOMO-LUMO overlaps. In some cases, orbital mismatch can be relieved by simple conformational changes, such as unhindered rotation about single bonds. In those cases, the reactant adjusts the geometry to remove the steric impediment and the proposed reaction geometry should be altered correspondingly.

The *second step* is to check for steric hindrance by displaying isodensity surfaces and looking

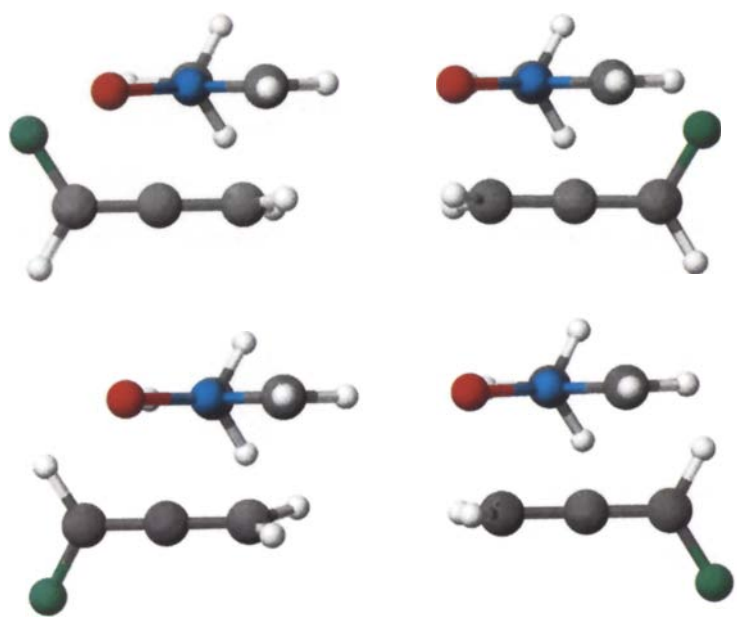

Fig. 20. Four of the eight orientations for the attack of monofluoroallene on nitrone.

for regions where isodensity surfaces overlap. Adjustments to the configuration (such as simple translation or rotations of the reactant) which do not affect significantly the orbital overlap can be made. The presence of overlapping density surfaces can be used to eliminate reaction channels suggested by HOMO-LUMO docking.

In some cases, the steric hindrance can be relieved by simple conformational changes such as unhindered rotation about single bonds. In those cases, providing the relief of strain does not affect the orbital overlap, the reactant adjusts its geometry to remove the steric impediment and the model reaction geometry should be altered correspondingly.

In the *third step*, electrostatic interactions are displayed and minimized as in the case of steric terms. The presence of overlapping electrostatic isopotential surfaces of the same sign can be used to eliminate reaction pathways suggested by HOMO-LUMO docking and allowed by steric interactions. The presence of overlapping electrostatic isopotential surfaces of different sign indicates that a reaction pathway suggested by HOMO-LUMO docking and allowed by steric interactions is very favorable.

In some cases, the electrostatic repulsion can be relieved by simple conformational changes such as unhindered rotation about single bonds. In those cases, providing the relief does not affect the orbital overlap, or induce steric repulsion, the reactant adjusts its geometry to remove the steric impediment and the model reaction geometry should be altered correspondingly.

Approximate transition states, built from structures along low-energy approach pathways, are excellent starting points for transition state searches.

An example: Why does the reaction of nitrone with monofluoroallene (MFA) favor the syn-*product?*

When nitrones attach to 1-fluoroallene (MFA), the predominant stereochemistry of these additions favors *syn*-attack on the allene [36]:

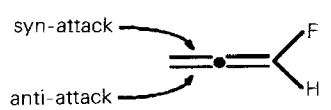

An example of this type of reaction, where 83% of the product is the *syn*, is the cycloaddition of *N*-*t*-butylnitrone to MFA:

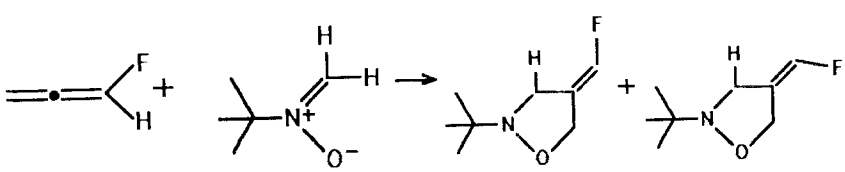

The observed *syn*/*anti* ratio is 3.6.

One possible explanation for the predominance of *syn* products is provided by the reactivity model described in the previous section. According to the reactivity model, when molecules react, three forces operate: (1) electron density on one reactant repels the electron density on the other (nonbonded, steric-like repulsion); (2) atoms with net positive charge in one reactant attract atoms with net negative charge in the other and repel atoms with net positive charge (electrostatic

interaction); and (3) occupied molecular orbitals on one reactant mix with unoccupied orbitals on the other (chemical bonding).

The following paragraphs present a qualitative explanation, based upon pictures of molecular surfaces, of why the *syn* addition product is preferred. The densities, electrostatic potentials and orbitals are all calculated for the reactants using the extended Hückel (EH) [37] method at minimum energy geometries*.

To explain the predominant product of the MFA-nitrone addition, begin with the chemical bonding term and the simple prototypical nitrone CH_3NOCH_2. The smallest HOMO-LUMO gap is between the LUMO on MFA and the HOMO on CH_3NOCH_2. The unoccupied orbital on MFA which is lowest in energy is an antibonding π-orbital between C_2 and C_3 and therefore, the appropriate orbital to describe the addition of the nitrone to MFA which breaks the C_2 and C_3 π-bond.

According to frontier orbital theory, nitrone can add to MFA when the HOMO on nitrone effectively overlaps the LUMO on MFA. Eight feasible pathways (see Fig. 20) which achieve good overlap of the HOMO and LUMO can be derived from the following three reactant orientations: (1) MFA can approach from above, or below, nitrone; (2) oxygen can bond to C_2 or C_3; and (3) F points toward, or away from, the nitrone. Of the eight cases, only two need to be considered. The orientations with O bonding to C_2 can be excluded because of repulsive electrostatic interactions between O and F which makes them energetically unfavorable and because they lead to the wrong products. The above and below approaches of MFA toward nitrone can also be excluded, because CH_3NOCH_2 is nearly planar and approach from above, or below, would obviously have similar orbital overlap and other interactions. Thus, the only two cases which must be considered are the approach of MFA from below the nitrone with O bonding to C_3 and F pointed toward (*syn* addition), or away from (*anti* addition), the nitrone.

Figures 21 and 22 show the docking of the LUMO (red and yellow) in MFA with the HOMO (blue and green) in the nitrone. In Fig. 21, MFA approaches from below the nitrone with the O bonding to C_2 and F pointing toward the nitrone (*syn* addition). Figure 22 shows a view similar to Fig. 21, but with the F pointing away from the nitrone (*anti* addition). Obviously, both overlaps are very similar and, solely on the basis of frontier orbital overlaps, both products would be expected with equal yield. The reason for the predominance of the *syn* product must lie in one of the other two interaction terms.

Figure 23 shows the 0.02 electron isodensities of MFA and nitrone docking at the same orientation and distance as in Fig. 21 (*syn* addition). Similarly, Fig. 24 shows the electron densities of MFA and the nitrone at the orientation of Fig. 22 (*anti* addition). The colors on the isodensity surfaces indicate the magnitude of the change of the electron density away from the isodensity surface. As can be seen, neither the *syn* nor the *anti* attack is sterically hindered or appears to have large nonbonded repulsion.

Figure 25 shows the electrostatic potentials of MFA and nitrone docking at the same orientation and distance as in Fig. 21 (*syn* addition). Similarly, Fig. 26 shows the electrostatic potentials of MFA and the nitrone at the orientation of Fig. 22 (*anti* addition). In these figures, the red surface is the +0.06 a.u. (37.65 kcal/mol or 157.5 kJ/mol) isopotential. The blue surface is the −0.06

* The minimum energy geometries were determined using the augmented MM2 force field in the CAChe™ Molecular Mechanics program V2.0, CAChe Group, Tektronix Inc., Beaverton, OR 97077, U.S.A.

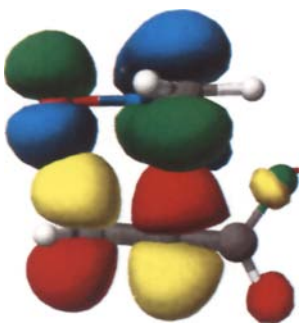

Fig. 21. HOMO-LUMO overlap during *syn* approach of monofluoroallene toward nitrone (0.05 a.u. isoamplitude).

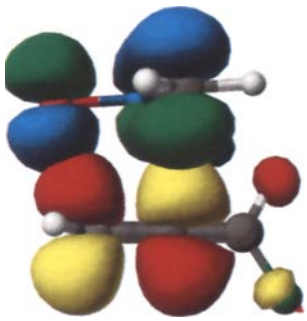

Fig. 22. HOMO-LUMO overlap during *anti* approach of monofluorallene toward nitrone (0.05 a.u. isoamplitude).

a.u. (37.65 kcal/mol or 157.5 kJ/mol) isopotential. Regions of space where positive surfaces on one reactant are near to or overlap negative surfaces on the other reactant are regions with attractive electrostatic interactions. Regions where surfaces of like potential overlap are regions with repulsive interactions.

As can be seen, in both orientations, the O–C_3 interaction is favorable, but the attractive F–CH_2 interaction in the *syn* geometry (Fig. 25) is clearly more favorable than the repulsive C_1–CH_2 interaction in the *anti* geometry (Fig. 26).

The structure shown in Fig. 21 is a graphically constructed, approximate transition state. It has been used as the starting point for an AM1 transition state search via the SADDLE method [38] in MOPAC. The search was successful. Figure 27 shows the resulting transition state as refined first with NLLSQ and then with a precise SIGMA calculation. A force calculation found only a single negative eigenvalue. Subsequent dynamic reaction coordinate calculations, in the direction defined by the eigenvector of this negative root, yielded the expected reactants and products. Note the striking similarity to the simple low-energy approach shown in Fig. 21. This example illustrates that approximate transition states, built from structures along low-energy approach pathways, are useful starting points for transition state searches.

Fig. 23. 0.02 a.u. electron isodensity overlap during *syn* approach of monofluoroallene toward nitrone.

Fig. 24. 0.02 a.u. electron isodensity overlap during *anti* approach of monofluoroallene toward nitrone.

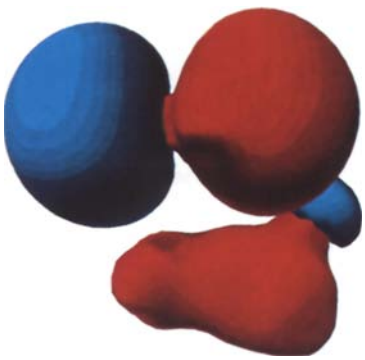

Fig. 25. 0.06 a.u. electrostatic isopotential overlap during *syn* approach of monofluoroallene toward nitrone.

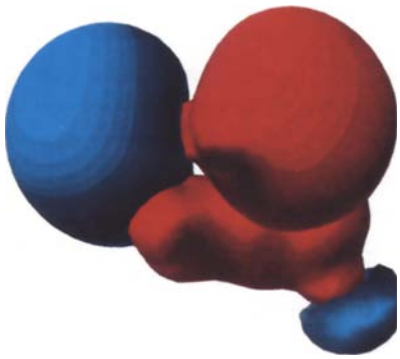

Fig. 26. 0.06 a.u. electrostatic isopotential overlap during *anti* approach of monofluoroallene toward nitrone.

The visual comparison of orbital overlap, electrostatic potentials and electron densities for the *syn* and *anti* approach, shows that only the electrostatic potential differentiates between the two approaches. This leads us to conclude that the reason the *syn* addition products predominate is electrostatic.

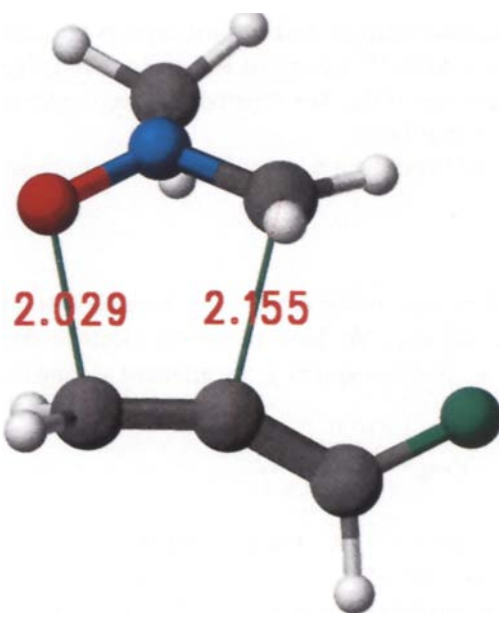

Fig. 27. The AM 1 transition state structure for the *syn* attack. Bond radii are proportional to the AM1 bond orders. The distances are in Å.

4. CONCLUSION

Novel insights into local molecule structure and reactivity can be gained from viewing isovalued surfaces of the molecular electron density, electrostatic potential and molecular orbitals rendered as colored, 3-D objects. For example, coloring isodensity surfaces to indicate the magnitude of the gradient of the electron density maps the molecule surface into regions of high and low electronegativity.

A basic understanding of reaction mechanisms can also come from viewing and manipulating isovalued surfaces. A theory of molecular interactions, based upon second-order perturbation theory, provides for the decomposition of the intermolecular interaction energy into steric, electrostatic and orbital interactions. At a particular reactant orientation, molecular isodensities, electrostatic isopotentials and orbitals can be displayed to visualize their contributions to the molecular interaction energy. These visualizations frequently reveal local interactions which determine the magnitude of the total interaction energy. This kind of insight is not easily obtained by simple evaluation of the total interaction energy. Low-energy reaction pathways can be surmised from displays of isovalued surfaces.

Computer visualization is never more useful than when it renders the unseeable, the unbuildable, or the unimaginable. Since individual electrons in molecules are unseeable, physical models of electron clouds are unbuildable and the quantized motion of electrons in their submicroscopic world are unimaginable, computer visualization attains its pinnacle when rendering the electronic structure of molecules.

5. ACKNOWLEDGEMENTS

As an illustration of the availability of desktop instruments for molecular engineering, this entire article was prepared on a CAChe™ Chemical Reactivity Modeling system from the CAChe™ Group at Tektronix, Beaverton, OR. The illustrations were printed at 300 dpi on a Tektronix 4693DX thermal transfer wax printer.

I thank Dr. Shi-Yi Liu for her critical review of the manuscript and constructive suggestions.

APPENDIX

There is also an interesting asymptotic relationship between the gradient of the electron density and the ionization potential: ε_{max}. At long range the electron density decreases like [39, 40]: $\lim_{r\to\infty} \rho(r) \sim e^{-2\sqrt{-2\,\varepsilon_{max}}r}$. Consequently, the gradient at long range behaves like:

$$\frac{\delta}{\delta r}\lim_{r\to\infty} \rho(r) \sim -2\sqrt{-2\,\varepsilon_{max}}\, e^{-2\sqrt{-2\,\varepsilon_{max}}\,r}$$

On an isodensity surface where $\rho(r)=C$, the gradient will be constant and proportional to the density with the proportionality of $-2\sqrt{-2\,\varepsilon_{max}}$. Thus, at long range, the gradient on an isodensity surface is proportional to the square root of the ionization potential.

Assume that the total molecular electron density can be approximated as a sum of atomic densities. Consider a molecular isodensity surface which is in the long-range region for each atom,

but which is not yet in the long-range region for the molecule as a whole. Then the gradient at any point on the surface will be proportional to the ionization potential of the atom nearest to that point. In other words, at long atomic distances – but inside of long-range molecular distances – the gradient of the electron density maps the variations in the square root of the local ionization potential of the molecule. A region with a large gradient indicates that electrons in that region are more tightly held than electrons in other regions where the gradient is smaller.

Since the spectroscopic electronegativity scale, based upon average valence shell ionization energy, parallels the Pauling electronegativity scale [41], the correlation between MNDO average gradient values for each element and Pauling electronegativity in Fig. 5 should cause no surprise. The single anomaly, hydrogen, is not unexpected. While the Pauling electronegativity scale places hydrogen between B and C, the Mulliken electronegativity scale places the electronegativity of hydrogen between N and O. The average gradient suggests that the electronegativity of hydrogen should be between that of C and N. Hydrogen is highly polarizable and the average hydrogen gradient in a molecule varies significantly depending upon the elements bonded to hydrogen. This is particularly apparent in extended basis ab initio calculations where the additional basis functions on hydrogen permit significant charge polarization [14].

REFERENCES

1 Lowdin, P.O., Phys. Rev., 97 (1955) 1974.
2 Bader, R.F.W., Henmeker, W.H. and Cade, P.E., J. Chem. Phys., 46 (1967) 3341.
3 Purvis III, G.D. and Culberson, J.C., J. Mol. Graphics, 4 (1986) 88.
4 Koide, A., Doi, A. and Kajioka, K., J. Mol. Graphics, 4 (1986) 149.
5 Hout, R.F., Pietro, W.J. and Hehre, W.J., A Pictorial Approach to Molecular Structure and Reactivity, John Wiley & Sons, New York, 1984.
6 See, for examples, Politzer, P. and Truhlar, D.G. (Eds.), Chemical Applications of Atomic and Molecular Electrostatic Potentials, Plenum Press, New York, 1981.
7 Jorgensen, W.L. and Salem, L., The Organic Chemist's Book of Orbitals, Academic Press, New York, 1973.
8 Stewart, J.J.P., MOPAC 5.10, CAChe™ Group, Tektronix, Inc., Beaverton, OR, 1989; Stewart, J.J.P., MOPAC 5.0, Quantum Chemistry Program Exchange, Program No. 455, Bloomington, IN, 1989.
9 (a)Dewar, M.J.S. and Thiel, W., J. Am. Chem. Soc., 99 (1977) 4899; (b) Dewar, M.J.S., J. Mol. Struct., 100 (1983) 41.
10 Huggins, M.L., J. Am. Chem. Soc., 75 (1953) 4126.
11 Weinstein, H., Politzer, P. and Srebrenik, S., Theoret. Chim. Acta (Berl.), 38 (1975) 159.
12 Purvis III, G.D. and Culberson, J.C., Int. J. Quant. Chem., QBS13 (1986) 261.
13 Purvis III, G.D., 1986, unpublished.
14 Sosa, C., Trucks, G.W., Purvis III, G.D. and Bartlett, R.J., J. Mol. Graphics, 7 (1989) 28.
15 Wiberg, K.B. and Walker, F.H., J. Am. Chem. Soc., 104 (1982) 5239.
16 Jackson, J.E. and Allen, L.C., J. Am. Chem. Soc., 106 (1984) 591.
17 Quarendon, P., Naylor, C.B. and Richards, W.G., J. Mol. Graphics, 2 (1984) 4.
18 Kahn, S.D., Pau, C.F., Chamberlin, A.R. and Hehre, W.J., J. Am. Chem. Soc., 109 (1987) 650.
19 Claverie, P., In Pullman, B. (Ed.), Intermolecular Interactions: From Diatomics to Biopolymers, John Wiley & Sons, New York, 1978.
20 Klopman, G., J. Am. Chem. Soc., 90 (1968) 223.
21 Salem, L., J. Am. Chem. Soc., 90 (1968) 543; loc. cit. 553.
22 Fleming, I., Frontier Orbitals and Organic Chemical Reactions, John Wiley & Sons, New York, 1976.
23 Mayer, A.I., Int. J. Quant. Chem., 23 (1983) 341.
24 Woodward, R.B. and Hoffman, R., The Conservation of Orbital Symmetry, Verlag Chemie, Weinheim/Bergstr., 1970.
25 Salem, L., Electrons in Chemical Reactions: First Principles, John Wiley & Sons, New York, 1982.

26 Albright, T.A., Burdett, J.K. and Whangbo, M.-H., Orbital Interactions in Chemistry, John Wiley & Sons, New York, 1985.
27 Teddar, J.M. and Nechvatal, A., Pictorial Orbital Theory, Pitman, London, 1985.
28 Fliszar, Charge Distributions and Chemical Effects, Springer-Verlag, New York, 1983.
29 Scrocco, E. and Tomasi, J., Adv. Quantum Chem., 11 (1978) 115.
30 Kollman, P.A., In Politzer, P. and Truhlar, D.G. (Eds.), Chemical Applications of Atomic and Molecular Electrostatic Potentials, Plenum Press, New York, 1981.
31 Streitwieser, Jr., A. and Owens, P.H., Orbital and Electron Density Diagrams, The Macmillan Company, New York, 1973.
32 Kahn, S.D. and Hehre, W.J., J. Am. Chem. Soc., 109 (1987) 663; ibid. 666.
33 Kahn, S.D., Pau, C.F. and Hehre, W.J., J. Am. Chem. Soc., 108 (1986) 7396.
34 Kahn, S.D., Pau, C.F., Overman, L.E. and Hehre, W.J., J. Am. Chem. Soc., 108 (1986) 7381.
35 Kahn, S.D. and Hehre, W.J., J. Am. Chem. Soc., 108 (1986) 7399.
36 Dolbier, Jr., W.R., Purvis III, G.D., Seabury, M.J., Wicks, G.E. and Burkholder, C.R., Tetrahedron, submitted.
37 Hoffmann, R., J. Chem. Phys., 39 (1963) 1397.
38 Dewar, M.J.S, Healy, E.F. and Stewart, J.J.P., J. Chem. Soc. Faraday Trans. II, 3 (1984) 227.
39 Morrell, M.M., Parr, R.G. and Levi, M, J. Chem. Phys., 62 (1975) 549.
40 Handy, N.C., Marron, M.T. and Silverstone, H.J., J. Phys. Rev., 45 (1969) 45.
41 Allen, L.C., J. Am. Chem. Soc., 111 (1989) 9003.